JHEP

Published for SISSA by Springer

Received: June 7, 2014
Accepted: July 25, 2014
Published: August 25, 2014

The windows for kinetically mixed Z'-mediated dark matter and the galactic center gamma ray excess

James M. Cline,[a] **Grace Dupuis,**[a] **Zuowei Liu**[a] **and Wei Xue**[b]

[a] *Department of Physics, McGill University,*
3600 Rue University, Montréal, Québec H3A 2T8, Canada
[b] *INFN — Sezione di Trieste and SISSA,*
via Bonomea 265, 34136 Trieste, Italy

E-mail: jcline@physics.mcgill.ca, dupuisg@physics.mcgill.ca, zuoweiliu@physics.mcgill.ca, xueweiphy@gmail.com

Abstract: One of the simplest hidden sectors with signatures in the visible sector is fermionic dark matter χ coupled to a Z' gauge boson that has purely kinetic mixing with the standard model hypercharge. We consider the combined constraints from relic density, direct detection and collider experiments on such models in which the dark matter is either a Dirac or a Majorana fermion. We point out sensitivity to details of the UV completion for the Majorana model. For kinetic mixing parameter $\epsilon \leq 0.01$, only relic density and direct detection are relevant, while for larger ϵ, electroweak precision, LHC dilepton, and missing energy constraints become important. We identify regions of the parameter space of m_χ, $m_{Z'}$, dark gauge coupling and ϵ that are most promising for discovery through these experimental probes. We study the compatibility of the models with the galactic center gamma ray excess, finding agreement at the 2-3σ level for the Dirac model.

Keywords: Beyond Standard Model, Cosmology of Theories beyond the SM

ArXiv ePrint: 1405.7691

doi:10.1007/JHEP08(2014)131

JHEP08(2014)131

Contents

JHEP08(2014)131

1 Introduction

A popular paradigm for dark matter (DM) models is that there exists a hidden sector [1, 2], including the dark matter particle and possibly many others, connected to the visible sector (the standard model, SM) by some weak "portal" interactions [3, 4]. Fermionic dark matter is theoretically attractive because its mass is protected by chiral symmetry and so does not introduce any new hierarchies of scale. It is natural to suppose that it has some gauge interactions in the hidden sector, of which the simplest possibility is U(1)$'$ (where the prime distinguishes it from the SM weak hypercharge). The portal is gauge kinetic mixing between the U(1)$'$ field strength $\tilde{Z}'_{\mu\nu}$ and the SM hypercharge $Y_{\mu\nu}$ [5]:

$$-\frac{\epsilon}{2}\tilde{Z}'_{\mu\nu}Y^{\mu\nu}. \tag{1.1}$$

One is then led to a simple and predictive model where there are only four essential parameters: ϵ, the U(1)$'$ gauge coupling g', and the masses m_χ, $m_{Z'}$ of the dark matter χ and the U(1)$'$ gauge boson Z'. Although there may be additional particles at a similar scale, such as a dark Higgs boson to give mass to the Z', it is not necessary to assume that they play an essential role, and it is consistent to consider the model with only four parameters. These can be constrained to a great extent by assuming a thermal origin for the DM relic density, and imposing constraints from direct searches for the DM and collider searches for the Z', as well as precision electroweak constraints.

The above statements are strictly true when the DM couples vectorially to the Z'. Another possibility is to have axial vector couplings, and so we consider both cases

$$\tilde{Z}'_\mu J^\mu_{\tilde{Z}'} = g' \bar{\chi} \gamma^\mu \tilde{Z}'_\mu \chi, \quad \frac{1}{2} g' \bar{\chi} \gamma^\mu \gamma_5 \tilde{Z}'_\mu \chi, \tag{1.2}$$

where χ is assumed to be a Dirac particle in the first case, and Majorana in the second. This is motivated by the fact that a Majorana fermion could have couplings only of the second type (though a Dirac fermion could have couplings of both types). We will refer to these two models as "Dirac" and "Majorana" dark matter. In the Majorana model we are obliged to also consider dependence upon the mass of the dark Higgs that is responsible for spontaneous breaking of the U(1)$'$, as will be explained.

This work aims to synthesize the most important constraints on kinetically mixed Z'-mediated dark matter models. Some aspects of our study are similar to previous ones [6]–[12], but with the exception of ref. [8], these papers study Z' models that are not just kinetically mixed but have additional interactions with the standard model. Ref. [8] focuses on electroweak precision constraints, while we incorporate in addition the constraints from relic density, direct detection and collider physics. Our analysis is distinctive in identifying the allowed parameter space in the well-motivated and economical hidden sector models where the mediation to the standard model is purely through gauge kinetic mixing.

We start in section 2 with a description of the models under consideration and a discussion of the extent to which they can be considered complete without reference to physics at higher scales. In section 3 the couplings of the Z' to standard model particles and to the DM are specified, as well as the visible and invisible decay widths of the Z'. Here we also briefly discuss electroweak precision constraints on the finely tuned region of parameter space where $m_{Z'} \cong m_Z$. Section 4 presents constraints from the relic density assuming that the DM is thermally produced. In section 5 we derive constraints coming from direct detection, while section 6 deals with those coming from dilepton searches at the LHC and precision electroweak studies. Sensitivity of missing energy signals (monojets) is also discussed. We synthesize the results in section 7, giving a summary of the regions of parameter space that are still allowed, as well as which experimental probes are most promising for discovery. In section 8 we discuss the potential for these models to address the galactic center gamma ray excess that has attracted attention recently. Conclusions are drawn in section 9, and details of cross section calculations are given in the appendices.

JHEP08(2014)131

2 Models

At the phenomenological level, the Dirac DM model is the simplest because the U(1)′ gauge symmetry does not prevent giving a mass to χ that is unrelated to spontaneous symmetry breaking. Moreover there need not be a Higgs field associated with the Z' mass; one can use the Stueckelberg mechanism [13] to directly give the Z' a mass. Hence it makes sense to consider the Dirac DM model as depending upon only the four parameters ϵ, g', m_χ, $m_{Z'}$. One indication of the consistency of this procedure is the fact that the DM annihilation cross section for $\chi\bar{\chi} \to Z'Z'$ has unitary behavior at large center of mass energy even if there is only χ exchange in the t-channel, with no need for Higgs exchange. The complete theory can be specified by the kinetic mixing (1.1) and the usual terms

$$\bar{\chi}(i\not{D} - m_\chi)\chi - \frac{1}{4}\tilde{Z}'_{\mu\nu}\tilde{Z}'^{\mu\nu} - \frac{1}{2}m^2_{Z'}\tilde{Z}'_\mu\tilde{Z}'^\mu \tag{2.1}$$

where $D_\mu = \partial_\mu - ig'\tilde{Z}'_\mu$ is the covariant derivative.

However for the Majorana DM model, it is not possible to have a bare mass term for χ consistent with the gauge symmetry; the Stueckelberg mechanism by itself would imply $m_\chi = 0$. To avoid this, we are obliged to consider spontaneous symmetry breaking, in which the dark Higgs boson h' cannot be much heavier than χ or Z' unless its self-coupling λ' is much greater than g' or the Yukawa coupling y' that gives rise to $m_\chi = y'\langle h'\rangle$. A consequence of this is that the cross section for $\chi\bar{\chi} \to Z'Z'$ violates unitarity at high energy unless the h' exchange diagram is included.

An ultraviolet complete version of the Majorana model is given by

$$\frac{1}{2}\sum_{i=1}^{2}\left[\bar{\chi}_i(i\not{\partial} \pm g'\gamma_5\not{\tilde{Z}}')\chi_i - y_i\bar{\chi}_i\left(\phi P_L + \phi^* P_R\right)\chi_i\right] + \left|(\partial_\mu - 2ig'\tilde{Z}'_\mu)\phi\right|^2 - V(\phi) \tag{2.2}$$

where the two Majorana fermions have charge $\pm g'\gamma_5$ to allow for anomaly cancellation, the scalar has charge $2g'$, and $P_{L,R} = \frac{1}{2}(1 \mp \gamma_5)$. A bare Dirac mass term $\bar{\chi}_1\chi_2$ can be forbidden by the discrete symmetry $\chi_1 \to \chi_1$, $\chi_2 \to -\chi_2$. Then after spontaneous symmetry breaking, we can consider the lighter of the two mass eigenstates $\chi_{1,2}$ to be the principal dark matter particle, while the heavier one (also stable) is subdominant, as we will verify when computing the relic density. This justifies the neglect of the extra DM component in our treatment.

3 Couplings and decays of Z'

The couplings of the Z' to standard model particles, via kinetic mixing, determine the visible contributions to the width of the Z' and the DM annihilation cross section, while the respective processes $Z' \to \chi\bar{\chi}$ or $\chi\bar{\chi} \to Z'Z'$ give the invisible contributions, if they are kinematically allowed. We distinguished (using the tilde) the interaction eigenstate $\tilde{Z}'_\mu$ of the U(1)′ boson that appears in eqs. (1.1), (1.2) from the corresponding mass eigenstate Z'_μ. Assuming that there is no mass mixing between Z and Z' other than that induced by

JHEP08(2014)131

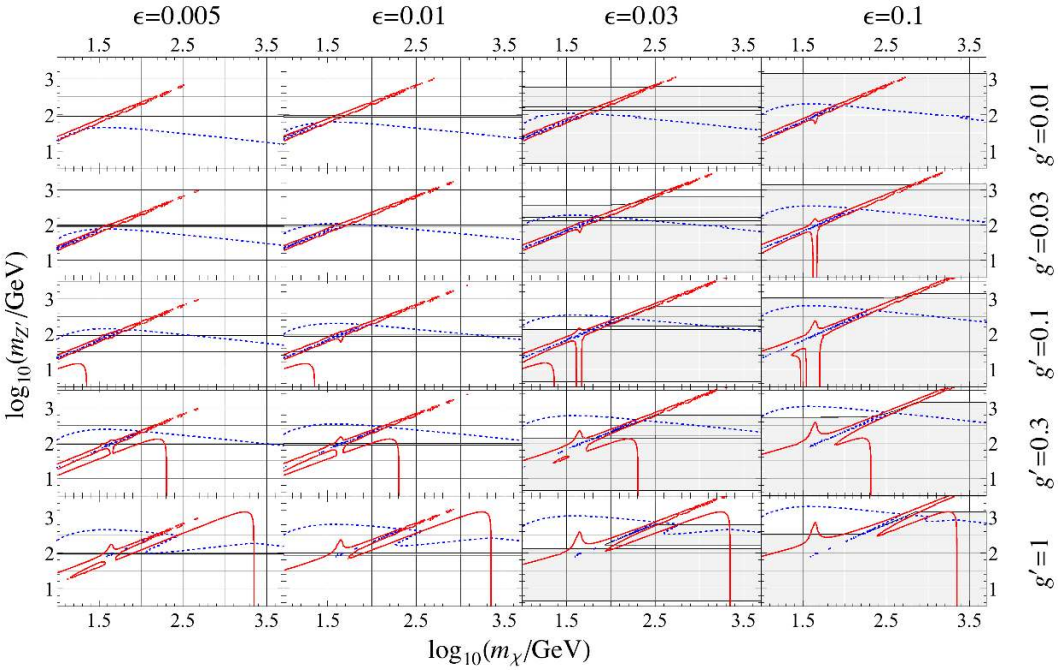

Figure 1. Solid (red) curves: relic density contours for the Dirac model in the m_χ-$m_{Z'}$ plane. ϵ varies from 0.005 to 0.1 (left to right) while g' varies from 0.01 to 1 (top to bottom). Dashed (blue) curves denote LUX direct detection upper limits on $m_{Z'}$. Shaded regions are excluded by ATLAS dilepton searches and precision electroweak constraints.

ϵ, the interaction Lagrangians for the physical Z and Z' are given by [7]

$$\begin{aligned}\mathcal{L}_{\rm int} = Z_\mu \left(-\epsilon c_W s_\zeta J^\mu_{\rm em} + (\epsilon s_W s_\zeta + c_\zeta) J^\mu_Z + s_\zeta J^\mu_{\tilde{Z}'}\right) \\ + Z'_\mu \left(-\epsilon c_W c_\zeta J^\mu_{\rm em} + (\epsilon s_W c_\zeta - s_\zeta) J^\mu_Z + c_\zeta J^\mu_{\tilde{Z}'}\right)\end{aligned} \tag{3.1}$$

where $c_W = \cos\theta_W$, $s_W = \sin\theta_W$, $c_\zeta = \cos\zeta$, $s_\zeta = \sin\zeta$, and we have assumed $\epsilon \ll 1$. The mass mixing angle ζ is given by

$$\tan(\zeta) = \frac{-\epsilon s_W m_Z^2}{m_{Z'}^2 - m_Z^2} \tag{3.2}$$

where m_Z represents the SM prediction for the Z boson mass.

In the Z' models considered here, the predicted value of m_Z gets shifted away from the SM value by an amount $\delta m_Z^2 = (m_{Z'}^2 - m_Z^2)\tan^2(2\zeta)$, which is constrained by precision electroweak data, namely the deviation $\delta\rho$ in the ρ parameter from its SM prediction $\rho = 1$. This leads to the constraint

$$\left|\frac{m_{Z'}^2 - m_Z^2}{m_Z^2}\right| > \frac{\epsilon s_W \delta\rho}{\delta\rho + 2\epsilon s_W} \tag{3.3}$$

where $|\delta\rho| < 10^{-3}$, conservatively. The maximum allowed value of $\tan(\zeta)$ is then of order $\delta\rho/\epsilon$.

JHEP08(2014)131

In the following we will focus on $\epsilon \geq 0.01$, for which ζ must therefore be small. For $m_{Z'} > m_Z$, it is then often adequate to approximate $c_\zeta = 1$, $s_\zeta = 0$. For smaller values of ϵ this approximation can break down, but only in a finely-tuned situation where $m_{Z'}$ is very close to m_Z. We will ignore this possibility in what follows. There are however a few situations where it is important to keep track of ζ more acccurately. One is when $m_{Z'} \ll m_Z$. In this regime, $\zeta \to s_W \epsilon$ and the coefficient $(\epsilon s_W c_\zeta - s_\zeta)$ in (3.1) that couples Z' to the Z current J_Z^μ is highly suppressed. We will see that this leads to a strong suppression of the spin-dependent cross section for scattering of Majorana DM on nucleons. A second such situation is the annihilation $\chi\chi \to f\bar{f}$ through the Z in the s-channel, where we keep $\sin\zeta \neq 0$ since the smallness of ζ can be compensated by the Z being nearly on shell in case of the accidental degeneracy $m_\chi \cong m_Z/2$, leading to resonant enhancement of the annihilation cross section.

Parametrizing the couplings of the Z and Z' to SM fermions as

$$\sum_i \bar{\psi}_i \left[\not{Z} \left(v_{i,Z} - a_{i,Z}\gamma_5 \right) + \not{Z}' \left(v_{i,Z'} - a_{i,Z'}\gamma_5 \right) \right] \psi_i \tag{3.4}$$

from (3.1) we find that

$$\begin{aligned}
v_{i,Z} &= c_\zeta \frac{e}{2c_W s_W}(T_{3,i} - 2s_W^2 Q_i) \\
a_{i,Z} &= c_\zeta \frac{e}{2c_W s_W} T_{3,i} \\
v_{i,Z'} &= -\epsilon c_W c_\zeta e Q_i + (\epsilon s_W c_\zeta - s_\zeta)\frac{e}{2c_W s_W}(T_{3,i} - 2s_W^2 Q_i) \\
a_{i,Z'} &= (\epsilon s_W c_\zeta - s_\zeta)\frac{e}{2c_W s_W} T_{3,i}
\end{aligned} \tag{3.5}$$

where Q_i is the electric charge and $T_{3,i}$ is the weak isospin. We have ignored corrections of $O(\epsilon^2)$ here. If $m_{Z'} \gg m_t$ and $\zeta \ll 1$, we can approximate the width of the Z' decaying into SM particles as

$$\begin{aligned}
\Gamma_{\text{SM}} &= \frac{m_{Z'}}{4\pi}\left(v_{e,Z'}^2 + v_{\nu,Z'}^2 + a_{e,Z'}^2 + a_{\nu,Z'}^2 + 3(v_{u,Z'}^2 + v_{d,Z'}^2 + a_{u,Z'}^2 + a_{d,Z'}^2)(1 + \alpha_s/\pi) \right) \\
&= \frac{\epsilon^2 \alpha m_{Z'}}{4c_W^2}\left(3 + \frac{11}{3}(1 + \alpha_s/\pi) \right)
\end{aligned} \tag{3.6}$$

The contribution from the top quark should be corrected by the factor $(1 + \frac{7}{17}x)\sqrt{1-4x}$ where $x = (m_t/m_{Z'})^2$ if x is not negligible. If $m_{Z'} \ll m_Z$, as explained in the previous paragraph, we cannot approximate $\zeta \cong 0$ because of the suppressed coupling of Z' to J_Z^μ (due to the factor $\epsilon s_W c_\zeta - s_\zeta$). In that regime, Z' couples to SM fermions only through the electromagnetic current, and we find that Γ_{SM} is smaller by the factor $4c_W^4/3$ relative to (3.6).

The invisible width due to $Z' \to \chi\chi$ is given by

$$\Gamma_{\text{inv}} = \frac{g'^2 c_\zeta^2}{12\pi\, m_{Z'}}\left(1 - \frac{4m_\chi^2}{m_{Z'}^2}\right)^{1/2} \begin{cases} m_{Z'}^2 + 2m_\chi^2, & \text{Dirac} \\ \frac{1}{2}m_{Z'}^2 - 2m_\chi^2, & \text{Majorana} \end{cases}$$

assuming that $m_{Z'} > 2m_\chi$.

JHEP08(2014)131

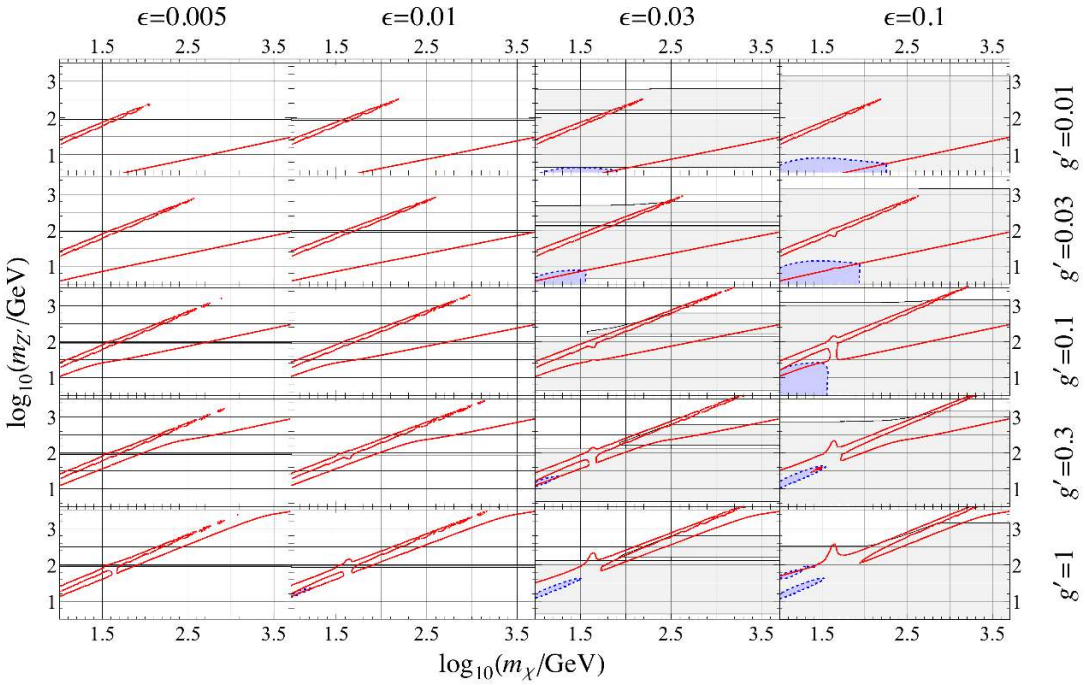

Figure 2. Relic density, direct detection and collider constraints for the Majorana model, as in figure 1. Dark (blue) shaded regions bounded by the dashed curves are excluded by LUX constraint on SI scattering. The dark Higgs mass is taken to be $m_\phi = m_\chi$.

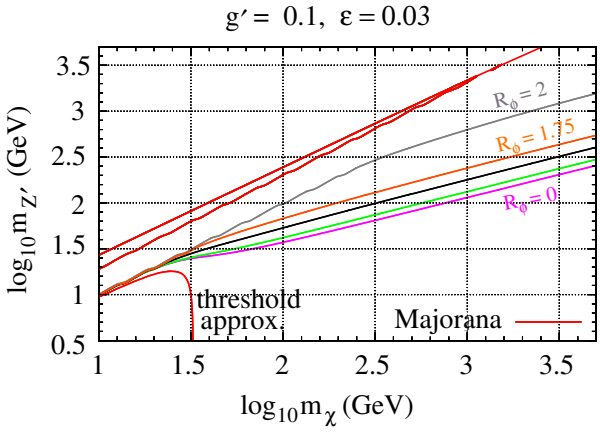

Figure 3. Allowed relic density contours for the Majorana model, with $g' = 0.1$, $\epsilon = 0.03$. Lowest curve uses the threshold approximation (evaluating cross section at $s = 4m_\chi^2$ and omitting the thermal average) for the $\chi\chi \to Z'Z'$ contribution to the cross section, rather than the thermal average of $\sigma v_{\rm rel}$. Upper curves show the effect of varying the dark Higgs mass on the Majorana relic density contours; $R_\phi = m_\phi/m_\chi$ varies between 0 and 2.

4 Relic density

There are two potentially important processes for determining the DM thermal relic density: $\chi\bar{\chi} \to f\bar{f}$, where f is any SM fermion coupling to Z' (the contribution from W^+W^- final states turns out to be negligible), and $\chi\bar{\chi} \to Z'Z'$ in the case where $m_\chi > m_{Z'}$.

JHEP08(2014)131

The corresponding processes $\chi\bar{\chi} \to f\bar{f}f\bar{f}$ or $\chi\bar{\chi} \to f\bar{f}Z'$, where one or both of the Z's is off-shell, turn out to give negligible contributions to the annihilation. Annihilations into Z bosons can only be important where s_ζ is so large that electroweak precision constraints are violated. We give details of the cross section calculations in appendices A–C.

To determine the relic density we have solved the full Boltzmann equation as well as using the accurate approximation described in ref. [19]. We find that a faster and accurate enough method is to compute the thermally averaged cross section $\langle\sigma v_{\rm rel}\rangle$ at the temperature $T = m_\chi/20$ and compare it to the standard value $(\sigma v)_{\rm th}$ needed for getting the right relic density. This quantity has been accurately determined as a function of m_χ in ref. [20]. Then the ratio of the χ relic density to that measured by WMAP7 ($\Omega_{\rm CDM}h^2 = 0.112 \pm 0.006$) is given by

$$f_{\rm rel} = \frac{g_\chi}{2}\frac{(\sigma v)_{\rm th}}{\langle\sigma v_{\rm rel}\rangle} \tag{4.1}$$

where $g_\chi = 4(2)$ for Dirac (Majorana) DM.

We display contours for $f_{\rm rel} = 1$ in the m_χ-$m_{Z'}$ plane for the two models (Dirac and Majorana DM) in figures 1 and 2, for a range of g' and ϵ. In nearly all cases, the observational uncertainty in $\Omega_{\rm CDM}$ does not exceed the widths of the curves. There are generally two regions where $\langle\sigma v_{\rm rel}\rangle$ has the desired value: one near $m_{Z'} \cong 2m_\chi$, where $\chi\chi \to f\bar{f}$ is resonantly enhanced, and the second (visible for large enough values of g') where $m_{Z'} \cong m_\chi$ so that $\chi\chi \to Z'Z'$ is suppressed by lack of phase space. For Dirac DM, this second branch becomes vertical in the m_χ-$m_{Z'}$ plane at a sufficiently large value of m_χ, beyond which the cross section becomes too small (because of the suppression from the intermediate χ propagator in the t channel). However for Majorana DM, the cross section falls much more slowly as a function of m_χ, and so the lower branch continues to large values of m_χ in this model. This is related to the different behavior at large s (the Mandelstam invariant) in the two models, that was described in section 2.

The slow fall-off of $\sigma v_{\rm rel}$ with s in the Majorana model necessitates doing the full thermal average to find $\langle\sigma v_{\rm rel}\rangle$, rather than simply evaluating it at $s = 4m_\chi^2$ (the threshold approximation). In figure 3 we give an example (with $g' = 0.1$, $\epsilon = 0.03$) showing that the latter is a very bad approximation when m_χ starts to exceed a certain (g'-dependent) value. Similarly, the cross section for $\chi\chi \to Z'Z'$ is somewhat sensitive to the mass of the dark Higgs boson, since its contribution to the scattering is necessary for getting physically sensible results. Whereas we fixed $R_\phi = m_\phi/m_\chi = 1$ in figure 2, in figure 3 we display the dependence upon R_ϕ. There is a marked increase in the cross section starting at $R_\phi = 2$, since the dark Higgs can be produced resonantly in that case. It is worth noting that in this model, the Yukawa coupling y_1 that enters into the scattering matrix element is related to the gauge coupling by $y_1/g' = 2m_\chi/m_{Z'}$ since both χ and Z' get their mass from the VEV of ϕ.

As a point of consistency for the Majorana model, we require that the heavier of the two fermions (which was required for anomaly cancellation) makes a subdominant contribution to the overall relic density. The contributions to $\sigma v_{\rm rel}$ from the longitudinal polarizations of the Z' bosons scale as $m_\chi^2/m_{Z'}^4$, so that the relative abundance of the heavier species

JHEP08(2014)131

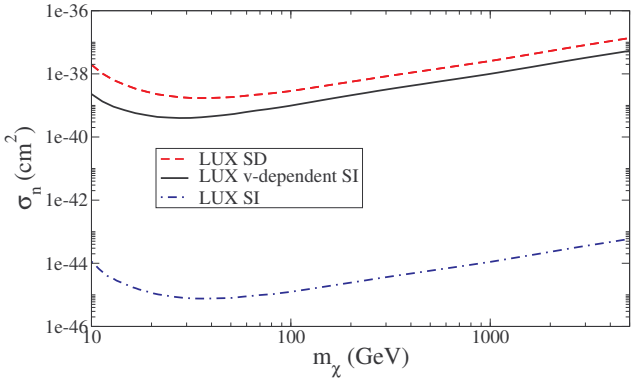

Figure 4. LUX limits on spin-independent, spin-dependent, and velocity-dependent nucleon cross sections, given respectively by eqs. (5.1), (5.3), (5.5). For the velocity-dependent case, $\hat{\sigma}_{\rm SI,M}$ is the constrained quantity.

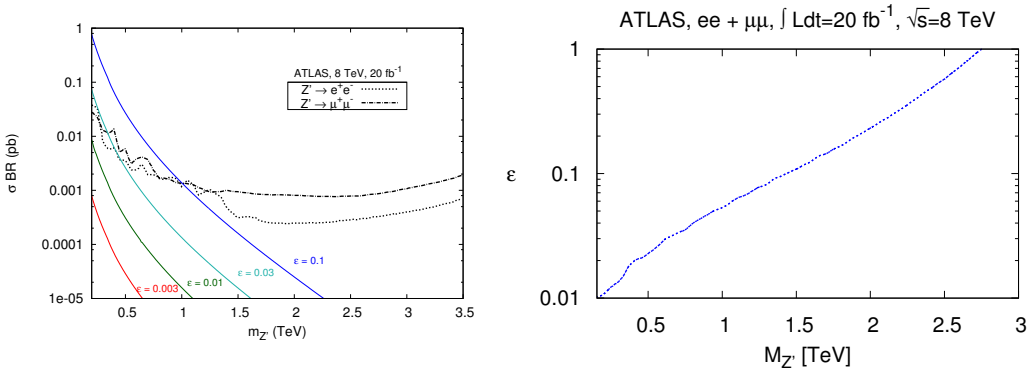

Figure 5. Left: LHC constraints on Z' models from dilepton resonances. Dashed curves: ATLAS limits on $\sigma B(Z' \to l^+l^-)$. Solid curves: dilepton production cross section as a function of the Z' mass for several values of ϵ. Right: upper bound on ϵ as a function of $m_{Z'}$ from ATLAS dilepton constraint, using combined electron and muon channels.

is suppressed by $(m_{\chi_1}/m_{\chi_2})^2$. We numerically verify this expectation in the high-m_χ, low-$m_{Z'}$ parts of the relic density contours that are associated with $\chi\chi \to Z'Z'$.

5 Direct detection

The cross section for spin-independent (SI) scattering of Dirac DM χ to scatter on nucleons at zero velocity is given by

$$\sigma_{\rm SI,D} = \frac{\mu^2}{\pi}\left[\sum_{i=Z,Z'} \frac{Z_N v_{p,i} + (A_N - Z_N) v_{n,i}}{A_N\, m_i^2}\, v_{\chi,i}\right]^2 \tag{5.1}$$

where $\mu = m_p m_\chi/(m_p + m_\chi)$ is the reduced mass, and we have averaged over protons and neutrons to account for coherence, using the charge Z_N and atomic number A_N of the nucleus. The vector couplings of the Z and Z' to the proton and neutron are given by (3.5), which is also valid for nucleons because of the conserved vector current. The

JHEP08(2014)131

corresponding couplings to χ are $v_{\chi,Z} = s_\zeta g'$ and $v_{\chi,Z'} = c_\zeta g'$. Numerically, we find that the cross section is fit to a good approximation by

$$\sigma_{\rm SI,D} \sim 1.3 \times 10^{-30} {\rm cm}^2 (g'\epsilon)^2 (m_{Z'}/{\rm GeV})^{-4} \tag{5.2}$$

for xenon. However we use the more exact formula (5.1) to obtain the limits presented below.

For Majorana DM there is a SI contribution to the scattering due to the vector current at the nucleon, which is suppressed by the relative velocity, and has different mass dependence:

$$\begin{aligned} \sigma_{\rm SI,M} &= v_{\rm rel}^2 \, \frac{m_n^2 + 2 m_\chi m_n + 3 m_\chi^2}{2(m_\chi + m_n)^2} \, \sigma_{\rm SI,D} \\ &\equiv v_{\rm rel}^2 \, \hat{\sigma}_{\rm SI,M} \end{aligned} \tag{5.3}$$

where m_n is the nucleon mass. There is in addition a spin-dependent (SD) contribution for Majorana DM. We define an effective averaged cross section on nucleons as

$$\begin{aligned} \sigma_{\rm SD,M} &\equiv \left(\sqrt{\sigma_p} + \sqrt{\sigma_n}\right)^2 \\ &= \frac{3\mu^2}{\pi} \left[\left| \sum_i \frac{a_{p,i} a_{\chi,i}}{m_i^2} \right| + \left| \sum_i \frac{a_{n,i} a_{\chi,i}}{m_i^2} \right| \right]^2 \end{aligned} \tag{5.4}$$

The axial vector couplings are not simply related to those of the constituent quarks, instead being given by

$$\begin{aligned} a_{j,Z} &= e \, \frac{c_\zeta}{4 c_W s_W} (g_s + 2 g_A T_{3,j}) \\ a_{j,Z'} &= e \frac{\epsilon s_W c_\zeta - s_\zeta}{4 c_W s_W} (g_s + 2 g_A T_{3,j}) \end{aligned} \tag{5.5}$$

where $g_A = 1.27$ is the axial-vector coupling for neutron decay and $g_s = 0.19$ is the strange quark contribution, while $a_{\chi,i} = -v_{\chi,i}$. The actual SD cross section σ_N on xenon nuclei depends upon a different linear combination of $a_{p,i}$ and $a_{n,i}$, as described in appendix D; the combination $|a_{p,i}| + |a_{n,i}|$ is just a normalization factor in the definition of (5.5) that divides out in the physical σ_N. This procedure is consistent because of the fact that $a_{p,i}/a_{n,i} = -(g_A + g_s)/(g_A - g_s)$ regardless of i, a constraint we have imposed when computing the bound on $\sigma_{\rm SD,M}$.

The LUX direct detection limit can be applied directly to $\sigma_{\rm SI,D}$; however we allow for the possibility for χ to be a subdominant component of the total dark matter by weakening the constraint according to

$$\sigma_{\rm SI,D} < \frac{\sigma_{\rm SI,LUX}}{f_{\rm rel}} \tag{5.6}$$

(where $\sigma_{\rm SI,LUX}$ is the experimental upper limit) in regions of parameter space where $f_{\rm rel} < 1$, since the signal is expected to be reduced by this factor.[1] The corresponding constraints on

[1] We do not do so if $f_{\rm rel} > 1$ since these cases are ruled out anyway and they make the graphs harder to read by causing the direct detection limit to nearly coincide with the relic density curves in the case of resonantly enhanced annihilation.

JHEP08(2014)131

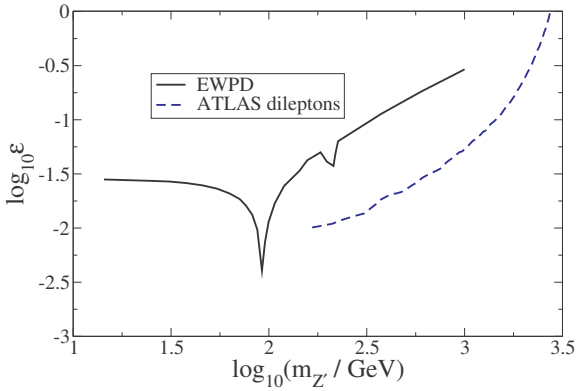

Figure 6. EWPD constraint on "wide" Z' from ref. [8], along with our constraint ϵ_0, eq. (6.1), from ATLAS dilepton searches.

$m_{Z'}$ are shown in figure 1 as the dashed (blue) curves. The use of (5.6) rather than the more common criterion $\sigma_{\rm SI,D} < \sigma_{\rm SI,LUX}$ that assumes $f_{\rm rel} = 1$ has the virtue that our exclusion curves indicate the true potential for direct detectability throughout the parameter space, rather than overestimating it.

For the velocity- and spin-dependent cross sections we must determine the limits on $\hat{\sigma}_{\rm SI,M} \equiv \sigma_{\rm SI,M}/v_{\rm rel}^2$ and $\sigma_{\rm SD,M}$ ourselves, by computing the corresponding cross sections on the Xe^{131} nucleus and comparing to the LUX data. Details are given in appendix D. The results are shown in figure 4.

For the Majorana DM model, we find that the limit on $\hat{\sigma}_{\rm SI,M}$ gives more stringent constraints than that on $\sigma_{\rm SD,M}$, despite the velocity suppression in the former.[2] This happens because the coefficient $(\epsilon s_W c_\zeta - s_\zeta)$ appearing in (5.5) is approximately zero for small $m_{Z'}$, making $a_{j,Z'} \cong 0$. For heavier $m_{Z'}$, the Z'-mediated contribution to the cross section is suppressed by $1/m_{Z'}^4$. (Although $(\epsilon s_W c_\zeta - s_\zeta)$ is also small in the SI cross section for the Dirac model, $v_{p,Z'}$ has an unsupressed contribution from the $-c_W c_\zeta Q_p$ term.) The corresponding limits on $m_{Z'}$ in the Majorana DM model are given by the dashed (blue) curves in figure 2, with dark (blue) shading indicating the excluded regions.

6 Collider constraints

There are constraints on the coupling of Z' to leptons from the processes $pp \to Z' \to e^+e^-, \mu^+\mu^-$ [18]. These were derived for other Z' models than the one considered here, so we have reanalyzed the ATLAS data to constrain the purely kinetically mixed Z', as described in appendix E. In figure 5(a) we show the limits on σBR for $Z' \to e^+e^-$ and $Z' \to \mu^+\mu^-$, where BR denotes the branching ratio for Z' to decay into these final states. Assuming that there are no invisible decays, the predicted values of σBR for models with

[2]Stronger limits on SD scattering on protons in the sun have been obtained by neutrino detection experiments [21, 22]. These depend upon the efficiency of getting neutrinos from the decays of final state particles from $\chi\chi$ annihilation. We have checked that even with the most sensitive channels, the SD limits obtained are not competitive with the LUX SI limit on our Majorana DM model.

JHEP08(2014)131

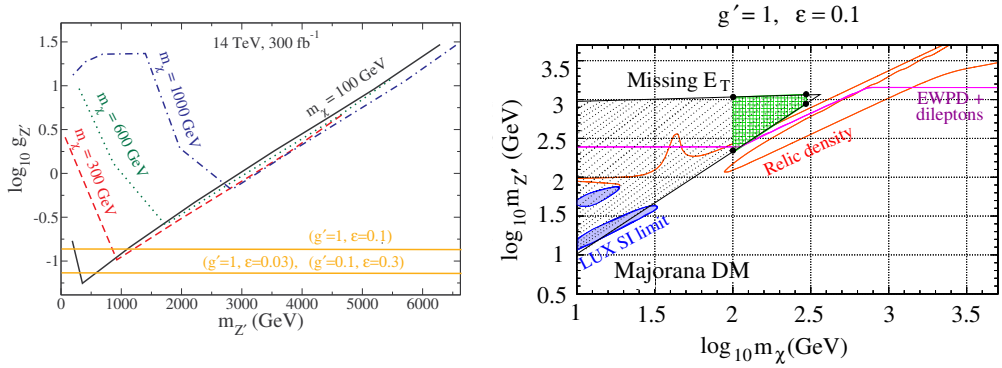

Figure 7. Left: projected LHC upper limits from missing transverse energy on $g_{Z'} = (0.175\, g'\epsilon)^{1/2}$ as a function of $m_{Z'}$ for several values of m_χ, adapted from ref. [23]. Horizontal lines denote the value of $g_{Z'}$ corresponding to the indicated values of g' and ϵ. Right: plot of the previous regions (labeled as "missing E_T") on the m_χ-$m_{Z'}$ plane for the Majorana model with $g' = 1$, $\epsilon = 0.1$, shown as (green) cross-hatched region. The (black) hatched region is an extrapolation of results of [23] to lower m_χ.

a given value of ϵ are also shown there. This allows us to derive the upper bound $\epsilon_0(m'_Z)$ as a function of Z', assuming that Z' decays only into SM fermions with the width $\Gamma_{\rm SM}$ given by (3.6). The function $\epsilon_0(m'_Z)$ is shown in figure 5(b).

In general, the above limit must be corrected for the invisible decays $Z' \to \chi\bar{\chi}$ through the branching ratio $BR_{\rm SM} = \Gamma_{\rm SM}/\Gamma_{\rm tot}$, where $\Gamma_{\rm tot} = \Gamma_{\rm SM} + \Gamma_{\rm inv}$, with $\Gamma_{\rm inv}$ given by (3.7). The general constraint is then given by

$$\epsilon < \frac{\epsilon_0(m_{Z'})}{(BR_{\rm SM})^{1/2}} \tag{6.1}$$

which depends upon both $m_{Z'}$ and m_χ.

The ATLAS limit extends only down to $m_{Z'} = 166\,\text{GeV}$. At lower masses, upper bounds on ϵ exist from electroweak precision data (EWPD) constraints [8]. We combine these with (6.1) to cover the range down to $m_{Z'} = 10\,\text{GeV}$. Generically, the dilepton and EWPD considerations are only relevant for $\epsilon \gtrsim 0.01$, with slightly more stringent constraints applying near $m_{Z'} = m_Z$ and other narrow mass regions in the case where $\Gamma_{\rm inv}$ is small. We adopt the "wide" Z' limit of ref. [8], replotted here in figure 6. For comparison our limit ϵ_0 is also plotted there. It should be kept in mind that even though ϵ_0 is lower than the EWPD limit in the region where they overlap, EWPD can be more stringent if $BR_{\rm SM}$ is sufficiently small.

A third collider signal for dark matter models such as those considered here is missing transverse energy which could occur in the on-shell production of the Z' if it decays invisibly into $\chi\bar{\chi}$. Initial state radiation from the incoming quarks could lead to monophotons or monojets. The ultimate sensitivity of LHC to Z' models similar to ours has been estimated in ref. [23], where projected constraints on the couplings of the Z' have been computed as a function of $m_{Z'}$ for $m_\chi = 100$ and $1000\,\text{GeV}$. In particular, the effective coupling $g_{Z'} = \sqrt{g' g_q}$ is bounded, where g' is the coupling of Z' to χ, and g_q is its coupling to

JHEP08(2014)131

quarks. For our purposes, we take $g_q \cong \epsilon c_W (2e/3)$ corresponding to the up quark coupling; then $g_{Z'} \cong (0.175\, g'\epsilon)^{1/2}$.

In figure 7(left), we reproduce the projected limits of [23] for the LHC at 14 TeV center-of-mass energy and 300 fb^{-1} integrated luminosity, including rough interpolations to indicate the limits at intermediate DM masses 300 and 600 GeV. For comparison, we draw horizontal lines corresponding to the largest values of $g'\epsilon = 0.1, 0.03$ considered in figures 1, 2. We see that the constraints are somewhat limited; for $g'\epsilon = 0.1$, $m_{Z'}$ is bounded only for $m_\chi \lesssim 300$ GeV, while for $g'\epsilon = 0.03$ the constraints disappear for $m_\chi \lesssim 100$ GeV. Nevertheless, they are complementary to other collider constraints, as shown in figure 7(right), where we translate the regions of monojet sensitivity shown previously to display them in the m_χ-$m_{Z'}$ plane, for the Majorana DM model with $g' = 1$, $\epsilon = 0.1$. Larger values of $m_{Z'}$ can be probed than those currently constrained by the dilepton and EWPD studies. The hatched region for $m_\chi < 100$ GeV is an extrapolation of the results taken from [23].

7 Allowed windows

In figures 1 and 2 we plot the contours for the relic density along with upper limits on $m_{Z'}$ from null direct detection searches, and the regions ruled out by dilepton and EWPD constraints. As has been noted in previous literature [11], the Dirac DM model (figure 1) is more highly constrained because of its typically larger cross section on nuclei. For small values of g', the only allowed regions are the ones where $\chi\chi$ annihilation into SM fermions is resonantly enhanced due to the accidental tuning of masses $m_\chi \cong m_{Z'}/2$. For $g'\epsilon \lesssim 5 \times 10^{-5}$, the direct detection constraint falls below the relic density curve along $m_\chi \cong m_{Z'}/2$, leaving all such models currently viable.

In the Dirac DM model, only for large values of the U(1)′ coupling $g' \sim 1$ does the competing channel $\chi\chi \to Z'Z'$ become strong enough to provide an alternative for satisfying both relic density and direct detection constraints. This window is largest for $\epsilon \lesssim 0.01$, below which direct detection and collider constraints are weakest. But it survives even for ϵ nearly as large as 0.1, at $m_\chi \cong 1.8$ TeV, $m_{Z'} \cong 1.4$ TeV. For $\epsilon > 0.03$, the collider/EWPD constraints become stronger than those from direct detection.

The Majorana DM model is less constrained because its cross section on nucleons is either spin-dependent or velocity suppressed. We found that the SI (but v-dependent) interaction gives the stronger limit. Even so, it hardly excludes any of the regions favored by the relic density. Only for $g' \sim 1$ and $m_\chi \sim m_{Z'} \sim 10$ GeV is there significant overlap of the direct detection and relic density curves. Like in the Dirac model, the relic density can be achieved either through $\chi\chi \to f\bar{f}$ (for $m_\chi \cong m_{Z'}/2$) or $\chi\chi \to Z'Z'$. But in contrast, the relic density contour due to the latter process extends to higher m_χ, due to the relatively larger contributions to the annihilation cross section from the emission of longitudinal gauge bosons. For $\epsilon \gtrsim 0.01$ the collider/EWPD bounds are more important that those for direct detection, giving the most promising means of discovery. For $g' \sim 1$, allowed regions with $m_\chi \sim m_{Z'} \sim$ several TeV exist even for ϵ as large as ~ 0.1.

JHEP08(2014)131

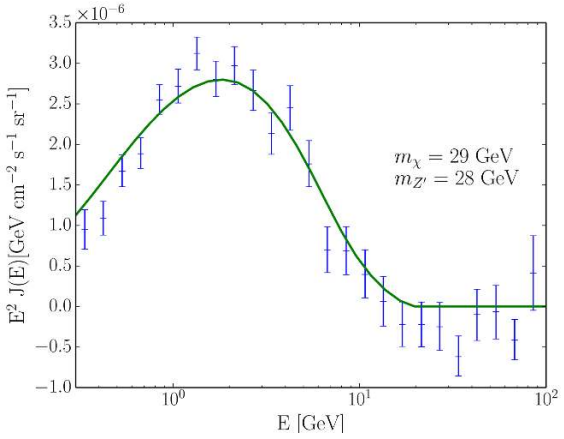

Figure 8. Spectrum of GC gamma ray excess; data are taken from ref. [26]; curve is the best-fit Dirac DM model prediction.

8 Galactic center gamma ray excess

Evidence from the Fermi Telescope has been found for excess 1-10 GeV gamma rays emanating from the galactic center (GC). Although millisecond pulsars may be a plausible source [24, 25], the possibility of dark matter annihilation has been vigorously pursued; for a recent discussion with references see [26]. Analyses of the data indicate that 40 GeV dark matter annihilating into $b\bar{b}$ provide a good fit to the signal [24].

Ref. [27] studied vector and axial-vector mediators in the s-channel, assuming only couplings to dark matter and to b quarks, showing that they are nearly ruled out as an explanation for the GC excess, by constraints from LUX direct detection and from CMS sbottom searches. On the other hand, refs. [28, 29] pointed out that these constraints are alleviated if $m_{Z'} < m_\chi$ so that $\chi\chi \to Z'Z' \to 4f$ (where f is a SM fermion) can proceed through on-shell Z' bosons in the GC. The coupling of Z' to $f\bar{f}$ can be much smaller in this case, since the on-shell Z' need only decay eventually into SM particles. Primarily g', m_χ and $m_{Z'}$ determine the strength of the GC signal, while the branching ratios of the decays into different final states affect the shape of the gamma ray spectrum.

We undertake a similar study here for the case where Z' couples to the SM through gauge kinetic mixing (this possibility was also considered in [28]). Since the models that give the best fit to the GC excess spectrum have light Z', the couplings of Z' to fermions are to a good approximation given by the $-\epsilon c_W c_\zeta e Q_i$ term in (3.5), *i.e.,* the Z' couples to their charges. We have generated the final photon spectrum using the Pythia-based results provided by ref. [30], which mainly considers the processes $\chi\chi \to f\bar{f}$ where each fermion has energy m_χ. To approximate the effect of 4-body final states, we convolve the photon spectra from a monoenergetic source with a box distribution,

$$\frac{\mathrm{d}N_\gamma}{\mathrm{d}E_\gamma} = \frac{2}{\delta m}\int_{(m_\chi-\delta m)/2}^{(m_\chi+\delta m)/2} \mathrm{d}m\, \frac{\mathrm{d}N_\gamma}{\mathrm{d}E_\gamma}(m) \tag{8.1}$$

where $\delta m \equiv \sqrt{m_\chi^2 - m_{Z'}^2}$ and $\frac{\mathrm{d}N_\gamma}{\mathrm{d}E_\gamma}(m)$ is the spectrum from a 2-body annihilation of particles with mass m. (The factor of 2 accounts for the decays of both Z's.)

JHEP08(2014)131

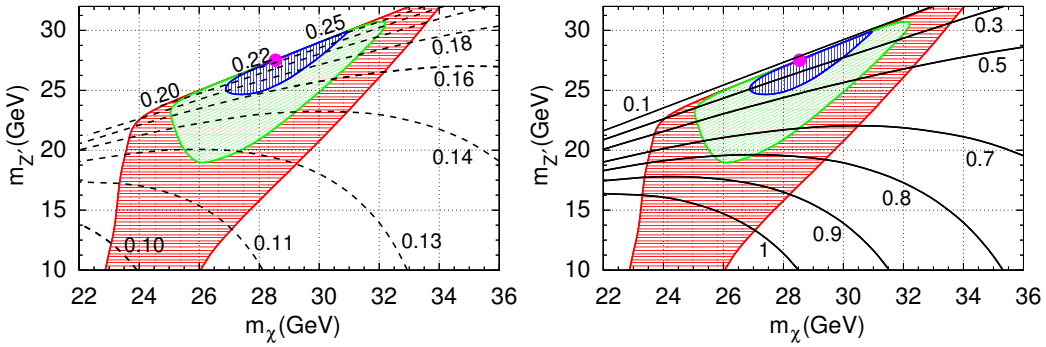

Figure 9. Shaded regions: 1σ, 2σ and 3σ confidence intervals for the galactic center gamma ray excess from cascade decays of $Z' \to f\bar{f}$ following $\chi\chi \to Z'Z'$. Dot (magenta) indicates best fit point. Dashed contours (left) are best-fit values of g'. Solid contours (right) give the fraction of the relic density $f_{\rm rel}$ for the Dirac DM model, assuming the g' values indicated on the left.

To relate the spectrum to the observed gamma-ray flux from the GC, we use the fact that in the galaxy the DM velocity is small, so that the zero temperature cross section (B.4) is applicable. The flux is given by

$$\frac{\mathrm{d}\Phi}{\mathrm{d}E_\gamma \mathrm{d}\Omega} = \frac{r_\odot}{4\times 4\pi}\left(\frac{\rho_\odot}{m_\chi}\right)^2 J\,\langle\sigma v\rangle_0 \frac{\mathrm{d}N_\gamma}{\mathrm{d}E_\gamma} \tag{8.2}$$

where the J factor is the integral along the line of sight

$$J = \int_{\rm l.o.s} \frac{\mathrm{d}s}{r_\odot}\left(\frac{\rho_\chi(r)}{\rho_\odot}\right)^2 \tag{8.3}$$

and $\langle\sigma v\rangle_0$ is the annihilation cross section at the kinematic threshold. We take for the local density at the sun $\rho_\odot = 0.3\,\mathrm{GeV/cm^3}$ and $r_\odot = 8.5\,\mathrm{kpc}$. We compare our theoretical prediction for the flux to the observed values reported in ref. [26], varying m_χ and $m_{Z'}$ which affect the shape of the spectrum, and adjusting g' at each $(m_\chi, m_{Z'})$ to obtain the best fit. We take ϵ to be negligibly small so that annihilations to $Z'Z'$ dominate over $f\bar{f}$ final states and direct detection and collider constraints are unimportant. The data and our model's fit to the spectral shape are shown in figure 8.

The resulting best-fit regions in the m_χ-$m_{Z'}$ plane are shown in figure 9, along with contours of the corresponding values of g' (left) and of the relic density fraction for the Dirac DM model $f_{\rm relic}$ (right). The best-fit point has $m_\chi \cong m_{Z'} \cong 28\,\mathrm{GeV}$, but the 3σ confidence region extends to low values of $m_{Z'} \sim 10\,\mathrm{GeV}$ and $m_\chi \sim 26\,\mathrm{GeV}$. The relic density is too low by a factor of ~ 6 at the best-fit point, but consistent with the observed value at the lower values of $m_{Z'} \sim 15\,\mathrm{GeV}$. (For the Majorana DM model, not shown here, the tension between the GC signal and the relic density is greater, due to the larger thermal annihilation cross section at the time of freeze-out, even though at threshold the two models have equal annihilation cross sections.) The discrepancy between $f_{\rm rel}$ and the parameters preferred for the GC excess may be ameliorated by taking into account astrophysical uncertainties [29], especially the possibility of a more concentrated DM halo profile, or accounting for part of the signal through millisecond pulsar emissions. Our allowed regions are similar to those found in ref. [31], though somewhat lower in the masses of χ and Z'.

JHEP08(2014)131

9 Conclusions

We have systematically studied the constraints from relic density, direct detection and collider experiments (dilepton production and electroweak precision data) on a simple dark sector, consisting of Dirac or Majorana dark matter, connected to the standard model by a kinetically mixed massive Z' gauge boson. The Dirac model can be considered to be UV (ultraviolet) complete, while the Majorana model is somewhat sensitive to details of the complete theory, such as the mass of the Higgs boson that spontaneously breaks the U(1)$'$ gauge symmetry, or the presence of an additional, heavier, subdominant DM component.

We have shown that the Dirac DM model requires the coincidence $m_\chi \cong m_{Z'}/2$ to get the right relic density if χ, and small values of $g'\epsilon$ to evade direct detection, if $m_\chi \lesssim 300\,\text{GeV}$. For heavier DM, there exist allowed models with larger values of $g'\epsilon$ where $\chi\chi \to Z'Z'$ determines the relic density, and χ could be discovered in future searches for scattering on nuclei or at colliders.

About the Majorana model, although it has some dependence upon extra parameters, the qualitative picture is clear: it much more easily escapes direct detection constraints except for strong couplings $g' \sim 1$ and small masses $m_\chi \sim m_{Z'} \sim 10\,\text{GeV}$. At large masses, only collider probes are sensitive, and then only for relatively large values of the kinetic mixing, $\epsilon \gtrsim 0.01$. In this regime, models with resonantly enhanced annihilation ($m_\chi \cong m_{Z'}/2$) are more likely to be compatible with the constraints, unless $g' \gtrsim 0.3$, in which case the more generic $\chi\chi \to Z'Z'$ branch of the relic-density-allowed regions (with lower values of $m_{Z'}$) can also be viable. This region may be discoverable not only through searches for dileptons but also monojets in the upcoming run of LHC.

Finally, we studied whether these models can explain the excess 1-10 GeV gamma ray signal from the galactic center found in data from the Fermi telescope. There is mild tension between the observed γ-ray signal and a thermal origin for the relic density, which is less severe in the Dirac model, and which would be less significant if the DM halo profile of the galaxy is more strongly peaked at the center, or if millisecond pulsars are responsible for part of the observed excess. The Dirac DM model is therefore an interesting candidate for the GC excess.

As we were completing this work, ref. [31] appeared, which also studied the viability of the light kinetically mixed Z' to explain the galactic center gamma ray excess.

Acknowledgments

We thank Guy Moore for pointing out the technique discussed in appendix C, Daniel Whiteson and Ning Zhou for helpful information about monojet searches, and Flip Tanedo and Tim Tait for correspondence about ref. [29].

A Cross section for $\chi\chi \to f\bar{f}$

The cross section for $\chi\chi \to f\bar{f}$ is given by

$$\sigma v_{\text{rel}} = 2\,g'^2\,F(s,\zeta,m_{Z'}) \begin{cases} \left(s + 2\,m_\chi^2\right), & \text{Dirac} \\ \left(s - 4\,m_\chi^2\right), & \text{Majorana} \end{cases} \tag{A.1}$$

where

$$F = c_\zeta^2\, BW(s,Z')\frac{\Gamma_{Z',\mathrm{SM}}}{m_{Z'}} + s_\zeta^2\, BW(s,Z)\frac{\Gamma_{Z,\mathrm{SM}}}{m_Z}$$
$$+2c_\zeta s_\zeta\left[(s-m_Z^2)(s-m_{Z'}^2) + m_Z m_{Z'}\Gamma_Z\Gamma_{Z'}\right]$$
$$\times BW(s,Z')\, BW(s,Z)\frac{\Gamma_{\mathrm{mixed}}}{(m_{Z'}m_z)^{1/2}} \tag{A.2}$$

and BW stands for the Breit-Wigner distribution $BW(s,m) = [(s-m^2)^2 + m^2\Gamma^2]^{-1}$ with Γ being the full width, whereas $\Gamma_{X,\mathrm{SM}}$ is the partial width for X to decay into SM fermions. The "mixed width" $\Gamma_{\mathrm{mixed}}/(m_{Z'}m_z)^{1/2}$ is defined in analogy to $\Gamma_{Z',\mathrm{SM}}/m_{Z'}$ in eq. (3.6), except one should replace $v_{x,Z'}^2 \to v_{x,Z'}v_{x,Z}$ and $a_{x,Z'}^2 \to a_{x,Z'}a_{x,Z}$.

To compute the thermal average of the annihilation cross section, it is convenient to define dimensionless variables $y = s/(4m_\chi^2)$ and $x = m_\chi/T$; the thermal average is then given by

$$\langle\sigma v_{\mathrm{rel}}\rangle = \frac{2x}{K_2^2(x)}\int_1^\infty dy\, y\sqrt{y-1}\, K_1(2x\sqrt{y})\,\sigma v_{\mathrm{rel}} \tag{A.3}$$

B Cross section for $\chi\chi \to Z'Z'$

For the Dirac DM model, σv_{rel} as a function of $y = s/(4m_\chi^2)$ and $R = m_{Z'}/m_\chi$ is

$$\sigma v_{\mathrm{rel}} = \frac{g'^4}{128\,\pi\, m_\chi^2}\left[\frac{Q_0Q_1 - Q_2Q_3Q_l}{y^{3/2}\sqrt{y-1}\,Q_d}\right] \tag{B.1}$$

where

$$\begin{aligned}
Q_0 &= 16\sqrt{y-1}\sqrt{y-R^2}(2y-R^2)\\
Q_1 &= (2+R^4+2y)\\
Q_2 &= -4R^2+R^4+4y\\
Q_3 &= 2(-2-2R^2+R^4+4y+4y^2)\\
Q_l &= \log\left[\frac{(R^2-2(y+\sqrt{y-1}\sqrt{y-R^2}))^4}{(-4R^2+R^4+4y)^2}\right]\\
Q_d &= (R^2-2y)(-4R^2+R^4+4y)
\end{aligned} \tag{B.2}$$

For the Majorana DM model, σv_{rel} also takes the form (B.1), but with

$$\begin{aligned}
Q_1 &= 16(1-y)(-4R^2+R^4+4y)(3R^4-4yR^2+4y^2)\\
&\quad -8(R_\phi^2-4y)(-4R^2+R^4+4y)(R^4-2yR^2+4y^2)\\
&\quad -(R_\phi^2-4y)^2\left[-R^8+2R^4(R^2+y)8(R^4-4yR^2+2y^2)\right]\\
Q_2 &= 2(4y-R_\phi^2)(-4R^2+R^4+4y)
\end{aligned}$$

$$
\begin{aligned}
Q_3 &= 8(R^2-2y)(-4R^4+R^6+8yR^2-8y^2) \\
&\quad +(R_\phi^2-4y)\left[16y(y-R^2)+4R^2(R^2-y)(R^2+4y)-R^4(R^4+4y^2)\right] \\
Q_d &= R^4(R^2-2y)(R_\phi^2-4y)^2(-4R^2+R^4+4y)
\end{aligned}
\tag{B.3}
$$

where $R_\phi = m_\phi/m_\chi$; ϕ is the dark sector Higgs boson that gives rise to $m_{Z'}$.

These cross sections at threshold are the same for Dirac and Majorana DM in the models under consideration:

$$
\sigma v_{\rm rel} = \frac{g'^4}{16\pi m_\chi^2}\, f(R), \quad f(R) \equiv \frac{(1-R^2)^{3/2}}{(1-\frac{1}{2}R^2)^2}
\tag{B.4}
$$

However we find that the thermally averaged values can differ significantly from the threshold values. This is especially true for the Majorana model, as described in section 4 (see figure 3.)

C Annihilation into 3 and 4 particles

To account for annihilations $\chi\chi \to Z'^* Z'^*$ into off-shell $Z's$, without explicitly doing the phase space integrals for the decay products, one can make the replacement

$$
2\pi \int \frac{d^4p}{(2\pi)^4}\,\theta(p_0)\,\delta(p^2-m^2) \quad \to \int \frac{d^4p}{(2\pi)^4}\,\theta(p_0)\,\theta(p^2)\,\frac{2\Gamma p_0}{(\Gamma p_0)^2+(p^2-m^2)^2}
\tag{C.1}
$$

in the usual invariant phase space integral for each final state Z', where the width is considered as a function of p_0. In the case that the decay products are approximately massless, $\Gamma = \hat{\Gamma} p_0$. If we label the energies of the off-shell Z's by E_3 and E_4, and their center-of-mass momenta as p, the cross section $\sigma v_{\rm rel}$ then becomes an integral over p, E_3 and E_4, with a delta function $\delta(\sqrt{s}-E_3-E_4)$. Rather than using this delta function to eliminate one of these integrals, it is convenient to save it for doing the integral over s in the thermal averaging. The result can be written as

$$
\begin{aligned}
\langle \sigma v_{\rm rel}\rangle = \frac{x}{2\pi^3 m_\chi^3 K_2^2(x)} \int_0^\infty dp\, p^2 \int_p^\infty dE_3 \int_p^\infty dE_4 \\
\times \langle|\mathcal{M}|^2\rangle \sqrt{y(y-1)}\, K_1(2x\sqrt{y})\,\theta(y-1) \prod_{i=3}^{4} \frac{\hat{\Gamma} E_i^2}{(\hat{\Gamma}E_i^2)^2+(p_i^2-m_{Z'}^2)^2}
\end{aligned}
\tag{C.2}
$$

where $y = (E_3+E_4)^2/(2m_\chi)^2$ and $p_i^2 = E_i^2 - p^2$.

To derive this, start with the Lorentz-invariant expression for $v_{\rm rel}$:

$$
v_{\rm rel} = \frac{2p_{1,\rm cm}}{E_{1,\rm cm}} = 4\frac{\sqrt{(p_1\cdot p_2)^2 - m_\chi^4}}{s}
\tag{C.3}
$$

Then

$$
d\sigma v_{\rm rel} = \frac{(2\pi)^4}{s}\langle|\mathcal{M}|^2\rangle\, d\Phi_2
\tag{C.4}
$$

JHEP08(2014)131

where

$$d\Phi_2 = \delta^{(4)}(p_i) \prod_{3,4} \frac{d^3 p_i}{(2\pi)^3 2E_i} \tag{C.5}$$

in the usual formulation. We modify the phase space according to

$$\frac{d^3 p}{(2\pi)^3 2E} \to 2 \frac{d^4 p}{(2\pi)^4} \frac{(\Gamma p^0)\,\theta(p^0)\,\theta(p^2)}{(\Gamma p^0)^2 + (p^2 - m^2)^2} \tag{C.6}$$

Substitution of the resulting $\sigma v_{\rm rel}$ into (A.3) results in (C.2).

Taking the limit $\hat{\Gamma} \to 0$ puts the final state Z's on shell and removes the integrals over E_i. Naively, it would seem valid to take this limit whenever the energy width of the thermal factor, which goes like $\exp((2m_\chi - E_3 - E_4)/T)$, is bigger than that of the Breit-Wigner factors. This is true when $T \gg \hat{m}_{Z'}$, or equivalently if freeze-out happens for $\hat{\Gamma} \ll m_\chi/(x_f m_{Z'})$. In our model, this implies we can put the Z's on shell as long as

$$\frac{m_{Z'}}{m_\chi} \ll \frac{1}{\epsilon^2} \tag{C.7}$$

in which case $\langle \sigma v_{\rm rel}$ does not depend upon ϵ. Otherwise it is necessary to do all three integrals and the result will be suppressed by some power of ϵ.

The above argument misses the cases where only one of the Z's is on shell, which dominate for some intermediate range of R. However in our numerical study we find that the 3- and 4-body channels make a small contribution to the total annihilation cross section, which we therefore ignore.

D LUX limit on SD and velocity-suppressed scattering

To compute the LUX spin-dependent (SD) scattering limit, the DM recoil rate is given by

$$\frac{\mathrm{d}R}{\mathrm{d}E_R} = \mathrm{Eff} \times \mathrm{Exp} \times N_T \frac{\rho_\oplus}{m_\chi} \int \mathrm{d}^3 v v f_\oplus(v) \frac{\mathrm{d}\sigma}{\mathrm{d}E_R}\,, \tag{D.1}$$

where N_T is the number of targets, $\rho_\oplus = 0.3\,\mathrm{GeV/cm^3}$, and the Maxwell-Boltzmann velocity distribution $f_\oplus(v)$ is assumed. The exposure Exp is (85 live days) $\times$ (118 kg) and the efficiency curve $\mathrm{Eff(E_R)}$ is provided by the LUX group. The DM-nucleus cross section rate gets contributions from two isotopes weighted by their abundances α_i, 21.8% for Xe^{131} and 26.2% for Xe^{129},

$$\frac{\mathrm{d}\sigma}{\mathrm{d}E_R} = \sum_{i=\binom{Xe^{131}}{Xe^{129}}} \alpha_i \sigma_{SD} \frac{m_N^2}{2\mu_N v^2} \frac{\mu_N^2}{\mu_n^2} \frac{4}{3} \frac{J+1}{J} \frac{\left(a_p \langle S_p \rangle + a_n \langle S_n \rangle\right)^2}{\left(|a_p| + |a_n|\right)^2} \Phi_i(q)\ . \tag{D.2}$$

We take the spin matrix elements of the neutron $\langle S_n \rangle$ and proton $\langle S_p \rangle$ from table I in [15]. For Xe^{131}, $J = 3/2$, $\langle S_n \rangle = -0.242$, $\langle S_p \rangle = -0.038$; for Xe^{129}, $J = 1/2$, $\langle S_n \rangle = 0.293$, $\langle S_p \rangle = 0.046$. Since we are considering a wide range of DM masses, and at large m_χ the momentum dependence makes an essential correction to the cross section, the two nuclear

JHEP08(2014)131

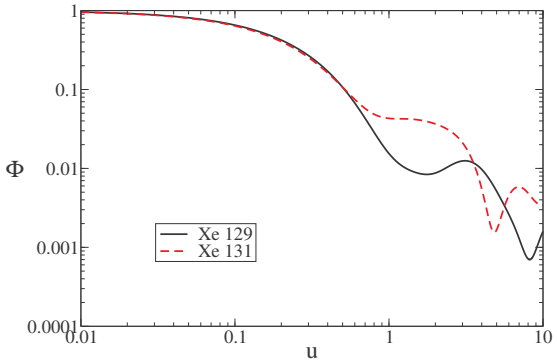

Figure 10. Form factors for spin-dependent scattering on Xe^{129} and Xe^{131} as a function of $u = q^2b^2/2$ (see text).

form factors $\Phi_i(q)$ for Xe^{131} and Xe^{129} are taken into account here [15]. Following ref. [16], we take the form factor for each element to be

$$\Phi_i(q) = \frac{g_A^2 S_{00}^{(i)}(q) + g_A g_s S_{01}^{(i)}(q) + g_s^2 S_{11}^{(i)}(q)}{g_A^2 S_{00}^{(i)}(0) + g_A g_s S_{01}^{(i)}(0) + g_s^2 S_{11}^{(i)}(0)} \tag{D.3}$$

The result is plotted in figure 10 as a function of $u \equiv q^2b^2/2$, where $q = \sqrt{2m_N E_R}$ is the momentum transfer and $b = 2.2853\,\text{fm}$ (2.2905 fm) for Xe^{129} (Xe^{131}).

For a given DM model, the predicted number of events is computed by integrating the recoil rate over the recoil energy from 3 keV_{nr} to 38 keV_{nr}. The upper limit of the DM cross section is derived by comparing the predicted number of events with the expected signal events, which ranges from 2.4 to 5.3 for different dark matter masses.

The rate for spin-independent (SI) scattering is also given by an expression of the form (D.1). The only difference relative to standard SI scattering in the case of the Majorana model is the extra dependence on v_{rel}^2 of (5.3), appearing in the phase space integral in (D.1).

E Dilepton production cross section

The predicted cross section for dilepton production at the LHC is given by

$$\frac{d\sigma(pp \to l^+l^-)}{dM} = K\frac{4M}{s}\int_1^\tau \frac{dx}{x} f_q(\tau) f_{\bar{q}}(\tau^2/x)\hat{\sigma}(q\bar{q} \to l^+l^-)$$

where M is the invariant mass of the lepton pair, $\sqrt{s} = 8\,\text{TeV}$ is the LHC hadronic centre of mass energy, for the relevant ATLAS constraints we consider, $f_{q,\bar{q}}(x)$ are the parton distribution functions, and $\tau = M^2/s$. The sum over quarks is implicit. We include a K-factor to account for next-to-leading-order corrections, which we take as $K = 1.5$ for the purposes of our analysis.

The parton level cross section for the process, which proceeds via s-channel exchange of γ, Z, or Z', is given by

$$\hat{\sigma}(q\bar{q} \to l^+l^-) = \frac{1}{32\pi}\frac{\hat{s}}{(\hat{s} - m_{Z'}^2)^2 + \Gamma_{Z'}^2 m_{Z'}^2}(v_{q,Z'}^2 + a_{q,Z'}^2)(v_{l,Z'}^2 + a_{l,Z'}^2)$$

JHEP08(2014)131

$$
\begin{aligned}
&+\frac{1}{16\pi}\frac{(\hat{s}-m_{Z'}^2)}{(\hat{s}-m_{Z'}^2)^2+\Gamma_{Z'}^2 m_{Z'}^2}\times \\
&\left(\frac{\hat{s}(\hat{s}-m_Z^2)}{(\hat{s}-m_Z^2)^2+\Gamma_Z^2 m_Z^2}(v_{q,Z}v_{q,Z'}+a_{q,Z}a_{q,Z'})(v_{l,Z}v_{l,Z'}+a_{l,Z}a_{l,Z'})\right. \\
&\qquad\left.-4e^2 Q_q v_{q,Z'} v_{l,Z'}\right) \\
&+\frac{1}{2\pi}\left(\frac{e^4 Q_q^2}{\hat{s}}-\frac{e^2 Q_q}{2}\frac{\hat{s}-m_Z^2}{(\hat{s}-m_Z^2)^2+\Gamma_Z^2 m_Z^2}v_{l,Z}a_{l,Z}\right. \\
&\qquad\left.+\frac{1}{16}\frac{\hat{s}}{(\hat{s}-m_Z^2)^2+\Gamma_Z^2 m_Z^2}(v_{q,Z}^2+a_{q,Z}^2)(v_{l,Z}^2+a_{l,Z}^2)\right)
\end{aligned}
\tag{E.1}
$$

The couplings of the Z and Z' to SM fermions, $v_{f,X}$ and $a_{f,X}$, are as given in eq. (3.5). The Z' width, $\Gamma_{Z'}$ is taken to be the decay width to SM particles, as given by eq. (3.6). We determine the branching ratio to leptons, using the partial width

$$
\Gamma(Z' \to l^+ l^-) = \frac{5\alpha\epsilon^2 M_{Z'}}{24 c_W^2} \tag{E.2}
$$

where $l = e$ or μ.

We determine the quantity $\sigma BR(Z' \to l^+ l^-)$ as a function of the Z' mass, for several choices of the kinetic mixing parameter, ϵ. Our result is shown in figure 5. From this constraint, we further determine an upper limit on ϵ as a function of $m_{Z'}$, equating our predicted cross section to the expected ATLAS limit, in the combined channel $e^+e^- + \mu^+\mu^-$. The result is shown in figure 6.

References

[1] M.J. Strassler and K.M. Zurek, *Echoes of a hidden valley at hadron colliders*, *Phys. Lett.* **B 651** (2007) 374 [hep-ph/0604261] [INSPIRE].

[2] M.J. Strassler, *Possible effects of a hidden valley on supersymmetric phenomenology*, hep-ph/0607160 [INSPIRE].

[3] M. Pospelov, A. Ritz and M.B. Voloshin, *Secluded WIMP dark matter*, *Phys. Lett.* **B 662** (2008) 53 [arXiv:0711.4866] [INSPIRE].

[4] N. Arkani-Hamed, D.P. Finkbeiner, T.R. Slatyer and N. Weiner, *A theory of dark matter*, *Phys. Rev.* **D 79** (2009) 015014 [arXiv:0810.0713] [INSPIRE].

[5] B. Holdom, *Two* U(1)*'s and epsilon charge shifts*, *Phys. Lett.* **B 166** (1986) 196 [INSPIRE].

[6] E. Dudas, Y. Mambrini, S. Pokorski and A. Romagnoni, *(In)visible Z-prime and dark matter*, *JHEP* **08** (2009) 014 [arXiv:0904.1745] [INSPIRE].

[7] S. Cassel, D.M. Ghilencea and G.G. Ross, *Electroweak and dark matter constraints on a Z-prime in models with a hidden valley*, *Nucl. Phys.* **B 827** (2010) 256 [arXiv:0903.1118] [INSPIRE].

JHEP08(2014)131

[8] A. Hook, E. Izaguirre and J.G. Wacker, *Model independent bounds on kinetic mixing*, *Adv. High Energy Phys.* **2011** (2011) 859762 [arXiv:1006.0973] [INSPIRE].

[9] A. Alves, S. Profumo and F.S. Queiroz, *The dark $Z^{'}$ portal: direct, indirect and collider searches*, *JHEP* **04** (2014) 063 [arXiv:1312.5281] [INSPIRE].

[10] G. Arcadi, Y. Mambrini, M.H.G. Tytgat and B. Zaldivar, *Invisible Z' and dark matter: LHC vs LUX constraints*, *JHEP* **03** (2014) 134 [arXiv:1401.0221] [INSPIRE].

[11] O. Lebedev and Y. Mambrini, *Axial dark matter: the case for an invisible Z'*, arXiv:1403.4837 [INSPIRE].

[12] A. Pierce and Z. Zhang, *Hidden dipole dark matter*, *Phys. Rev.* **D 90** (2014) 015026 [arXiv:1405.1937] [INSPIRE].

[13] B. Körs and P. Nath, *A Stueckelberg extension of the standard model*, *Phys. Lett.* **B 586** (2004) 366 [hep-ph/0402047] [INSPIRE].

[14] D. Perevalov, *Neutrino-nucleus neutral current elastic interactions measurement in MiniBooNE*, FERMILAB-THESIS-2009-47 (2009) [INSPIRE].

[15] M. Cannoni, *Reanalysis of nuclear spin matrix elements for dark matter spin-dependent scattering*, *Phys. Rev.* **D 87** (2013) 075014 [arXiv:1211.6050] [INSPIRE].

[16] J. Menendez, D. Gazit and A. Schwenk, *Spin-dependent WIMP scattering off nuclei*, *Phys. Rev.* **D 86** (2012) 103511 [arXiv:1208.1094] [INSPIRE].

[17] S. Yellin, *Finding an upper limit in the presence of unknown background*, *Phys. Rev.* **D 66** (2002) 032005 [physics/0203002] [INSPIRE].

[18] ATLAS collaboration, *Search for high-mass dilepton resonances in $20\,fb^{-1}$ of pp collisions at $\sqrt{s} = 8$ TeV with the ATLAS experiment*, ATLAS-CONF-2013-017 (2013).

[19] J.M. Cline, K. Kainulainen, P. Scott and C. Weniger, *Update on scalar singlet dark matter*, *Phys. Rev.* **D 88** (2013) 055025 [arXiv:1306.4710] [INSPIRE].

[20] G. Steigman, B. Dasgupta and J.F. Beacom, *Precise Relic WIMP abundance and its impact on searches for dark matter annihilation*, *Phys. Rev.* **D 86** (2012) 023506 [arXiv:1204.3622] [INSPIRE].

[21] IceCube collaboration, M.G. Aartsen et al., *Search for dark matter annihilations in the Sun with the 79-string IceCube detector*, *Phys. Rev. Lett.* **110** (2013) 131302 [arXiv:1212.4097] [INSPIRE].

[22] Baikal collaboration, A.D. Avrorin et al., *Search for neutrino emission from relic dark matter in the Sun with the Baikal NT200 detector*, arXiv:1405.3551 [INSPIRE].

[23] N. Zhou, D. Berge, L. Wang, D. Whiteson and T. Tait, *Sensitivity of future collider facilities to WIMP pair production via effective operators and light mediators*, arXiv:1307.5327 [INSPIRE].

[24] K.N. Abazajian, N. Canac, S. Horiuchi and M. Kaplinghat, *Astrophysical and dark matter interpretations of extended gamma-ray emission from the galactic center*, *Phys. Rev.* **D 90** (2014) 023526 [arXiv:1402.4090] [INSPIRE].

[25] Q. Yuan and B. Zhang, *Millisecond pulsar interpretation of the Galactic center gamma-ray excess*, *JHEAp* **3-4** (2014) 1 [arXiv:1404.2318] [INSPIRE].

[26] T. Daylan et al., *The characterization of the gamma-ray signal from the central Milky Way: a compelling case for annihilating dark matter*, arXiv:1402.6703 [INSPIRE].

JHEP08(2014)131

[27] E. Izaguirre, G. Krnjaic and B. Shuve, *The galactic center excess from the bottom up*, arXiv:1404.2018 [INSPIRE].

[28] A. Martin, J. Shelton and J. Unwin, *Fitting the galactic center gamma-ray excess with cascade annihilations*, arXiv:1405.0272 [INSPIRE].

[29] M. Abdullah et al., *Hidden on-shell mediators for the galactic center gamma-ray excess*, arXiv:1404.6528 [INSPIRE].

[30] M. Cirelli et al., *PPPC 4 DM ID: a Poor Particle Physicist Cookbook for Dark Matter Indirect Detection*, *JCAP* **03** (2011) 051 [*Erratum ibid.* **1210** (2012) E01] [arXiv:1012.4515] [INSPIRE].

[31] A. Berlin, P. Gratia, D. Hooper and S.D. McDermott, *Hidden sector dark matter models for the galactic center gamma-ray excess*, *Phys. Rev.* **D 90** (2014) 015032 [arXiv:1405.5204] [INSPIRE].

JHEP08(2014)131